2015 Tenth International Conference on Ecological Vehicles and Renewable Energies (EVER)

Hybrid Shipping for Inland Navigation: Loss Analysis of an Aluminum Direct-Drive High Performance 11,000Nm Permanent Magnet Machine

J.J.H. Paulides, N. Djukic and L. Encica
Advanced Electromagnetics BV, www.ae-grp.nl, the Netherlands
Email: info@ae-grp.nl

Abstract— **Hybrid electric ship propulsions are becoming a leading/emerging area of research, prompting investigation in hybrid propulsion system design and demonstration of concept vessels. With respect to ship design and operation, minimizing costs associated with fuel consumption and maintenance are key objectives. As such, new, and existing, ships are subject to regulatory requirements, especially regarding emissions and energy efficiency. Hybrid electric propulsion is a promising approach in addressing these concerns. Particularly for inland vessels that require a high degree of manoeuvrability and are continuously travelling upstream and downstream. In this work, a Permanent Magnet propulsion motor with 350kW at 300rpm, hence around 11,000Nm, will be discussed. With this motor a quiet mode is available with reduced emission during electric cruising and dynamic positioning.**

Keywords—***Hybrid propulsion, High Torque machines, Electric Powertrain, Synchronous motor, Brushless machine, Electric cruising.***

I. INTRODUCTION

The main advantages of the diesel-electric propulsion are its flexibility, resulting in better space utilization and higher redundancy, more economical operation, less maintenance and reduced environmental pollution. As such, diesel-electric propulsion is most popular in ships that are operated in partial load conditions for a significant portion of their time. For example, inland ship that require up- and down-stream operation. In these, the popularity of diesel-electric propulsion systems (0.5 – 1.5 MW range) is ever increasing, since potentially about 10-20% diesel can be saved on specific journeys [1, 2].

Electric machines, which can operate both as motor and generator, are already a well-established technology used due to their efficiency and reliability. Of course, also in shipping applications operating costs should be minimized, hence it is no surprise that fleet owners are considering a diesel-electric propulsion [3, 4].

Fig. 1. MTS Martinique, a single screwed pilot inland vessel with a hybrid propulsion system [5].

Future inland ships require power systems with improved fuel economy, hence reduced emission, while they are able to meet the power demand. With the use of power electronic converters, shipboard distribution systems can be supplied from a direct-drive shaft connected electric machine [6]. However, very little papers concern the specifics of the electric machine design for these diesel-electric propulsion system used for inland shipping applications.

The paper is organized in five Sections. In the second Section, the hybrid shipping concept will be presented in more detail. The third Section outlines the motor design and loss analysis and the fourth the thermal analysis. In the fifth Section, some implementation issues are highlighted and finally, in the sixth Section, conclusions are presented.

II. HYBRID SHIP

Almost all inland ships are equipped with a traditional propulsion systems based on an internal combustion engine. However, new ways are introduced to conceive propulsion and power systems for inland shipping. Within these propulsion solutions, medium-speed diesel or gas engines are connected to the propeller through a speed reducing transmission system. This is usually a reduction gear. Considering transmission losses means that for the

978-1-4673-6785-1/15/$31.00 ©2015 European Union

same propeller power, medium speed diesel engines must develop about 2 percent more power in the geared design [7]. However, various "hybrid propulsion" solutions are now considered for inland shipping:

- Parallel hybrid; medium-speed engine is the main energy source for propulsion (connected to the screw by a transmission) and a low speed electric machine is directly coupled to the screw or
- Series hybrid; medium-speed engine is run at constant speed and drives a generator. This generator creates the electric power to drive the low speed larger power electric machine which is directly coupled to the screw or
- Series-parallel hybrid; which is a combination of the two above-mentioned individual architects.

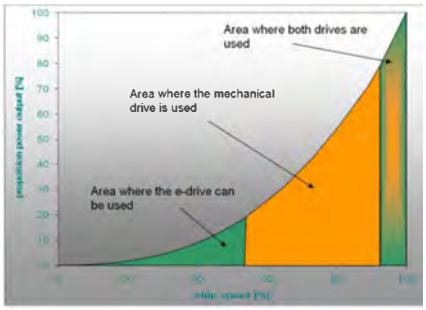

Fig. 2. Propulsion power to the screw versus ship percentage of speed, illustrating Generator, Electric cruise and Boost mode [8]

Each of these architects also have their alternatives. For example, series hybrid could also be when fuel cells (with or without on-board storage) are used to generate electric energy instead of engine-generator group [9, 10]). Parallel hybrid could be when an electric motor is only run when a peak propulsive power is required. However, this is almost never the case, since this does not allow for full electric cruising. Therefore, much more often a combination, series-parallel architecture, is utilized [11]. This allows for three modes (Fig. 2):

1. **Electric cruise mode**; at low speed, hence low power (<200-300kW) the boat is driven purely by the electric motor. Diesel-electric generator sets and/or battery pack are used to provide the energy for this electric cruising.
2. **Generator mode**; the hotel load is supplied and/or on-board battery pack is charged. This allows one or two generator sets to be switched off, since enough power can be generated in generator mode.
3. **Boost mode**; the middle speed range, depending on dynamic requirements, uses the Boost mode to support the combustion engine with the constant torque of the electric motor. An improved response of the propulsion occurs through the boost mode.

The resulting fuel efficiency depends on many variable, e.g. ship type (length, width, hull profile, etc.), trajectory (river, canals, depth, etc.) and load-cycle (frequency and magnitude of accelerations, duration of the stops, distances to be covered, etc.). However, on average this technology increases energy efficiency. For some specific journeys fuel savings can be even 25% [12]. Further this hybrid technology lowers the installed diesel propulsion power on a ship and also maintenance intervals of the main engine are prolonged. The fuel savings are also strongly influenced by energy management [13]. Especially when a micro grid (usually includes storage) is introduced, since power flows are directly related to mass, volume and cost of the installed energy storage [14].

Fig. 3. Illustrating 25% diesel fuel savings for 1 week of shipping on a specific journey [12].

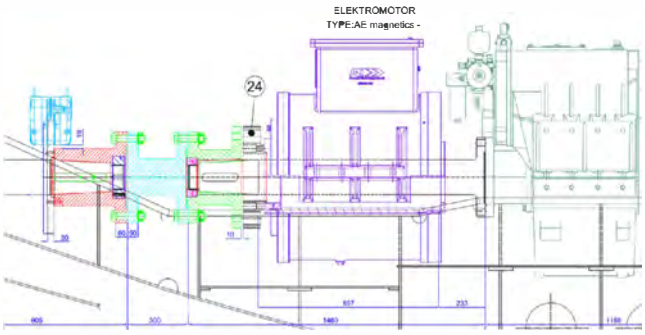

Fig. 4. Propulsion schematic hybrid ship [15]

Modern hybrid ships use one or two diesel or gas engines that (for engines >500kW) operated at 0-1,500 rpm. These are then connected via a gearbox as shown in Fig. 4. In all inland ship (hybrid or not), diesel/gas generator sets are also installed to provide power to the on-board electric grid, bow thrusters, etc. In a hybrid ship, in general, a direct-drive electrical machine is placed. These hybrid propulsion systems are especially used when the ship has relatively short trips in between ports, such as coastal tankers and containerships that operate in between European countries, ferries that make relatively short trips and ships that spend a great deal of

time manoeuvring, at harbour or cruising at variable speeds (e.g. in-land ships). Given that the relationship between speed and required power of a ship is cubic, the required power drops significantly when operating at lower speeds, as was shown in Fig. 2.

In this paper the focus will be on the electric machine that is installed in ships with a 0.5 – 1.5 MW propulsion system in which the diesel engine is the main engine. This electrical machine is connected to the ship's grid through an inverter. This inverter is, most commonly, a PWM voltage source inverter to supply the highly electric machine. This is particularly suitable for inland ships that often operate at partial load. As such, a highly efficient direct-drive electric machine will be designed that can be placed around the inland ship's propulsion shaft, as shown in Fig. 4.

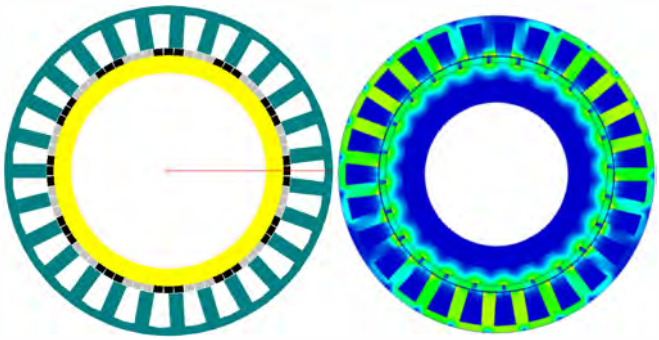

Fig. 5. Selected direct-drive motor configuration.

III. MOTOR ELECTROMAGNETIC DESIGN

Although specific electric machines can reach power density in the range of 6-12 kW/kg [16], this coincides with high speed operation. As the electric motor of the inland hybrid ship is placed around, and directly coupled to, the propulsion shaft, the operating speed is usually in the range of 0-450 rpm. Although specific machines could be designed for this application that uses multi-phase windings for lower harmonic content, the focus is on mere standard direct-drive three phase designs that can be operated with regular three leg inverters.

Table 1: Example of machine parameters

Machine:	Motor with external PM
Type:	PEMT -M-400-0325
Dimension drawing number:	051319-1401-A3-P00-A
Characteristics sheet number:	051319-1401-CN-001
Number of poles:	24
Stator winding connection:	Y
Direction of rotation (looking facing DE side of the shaft):	Both
Dyty cycle:	S1

Parameters data:

Value	Nominal
Power [kW]	210
Speed [rpm]	201
Frequency [Hz]	40.2
Voltage line-to-line [V]	267
Shaft torque [Nm]	10035
Efficiency [%]	94.60

Considering the inland ship environment, it was decided to use regular water as a cooling medium for the motor design. Preceding the motor design, the propulsion power versus ship speed has been determined, as was illustrated in Fig. 2. Following, an estimation is made on the required power range of the electric machine, as summarized in Table 1 for the electric cruising mode.

First, a motor configuration had to be selected that is capable to provide a high-efficiency at low-speeds and high-torques at a reasonable price. As such, an electrical machine containing permanent magnets has been selected with concentrated windings due to ease of manufacture (Fig. 5) [17]. Second, the operating envelope has been determined being 11,000 Nm nominal at 200 rpm with a constant torque to 345 rpm to allow augmentation of the diesel engine, hence this can be minimized in size. However, for a constant torque of 11,000Nm, the electric machine should also be able to achieve a speed of around 450 rpm. It needs noting that this maximum speed is given by the formula:

$$n_{\max} = \frac{60\ f}{p} = 450 \text{ rpm}$$

Where f is the fundamental frequency and p is the number of pole-pairs. For this application, we have limited the operational frequency to $f < 100$ Hz. Therefore the following is obtained:

$$p \le \frac{60 \cdot 100}{n_{\max}} = \frac{6000}{450} = 13.33 \text{ pole-pairs} \cdot$$

This selected frequency and speed impose a number of poles-pairs maximum equal to thirteen, i.e. this motor can be designed with maximum twenty-six poles. The proposed initial design has twenty-four poles and twenty-seven slots [18]. This combination is known to give a low cogging torque being a multiple of the nine slot / eight pole configuration. Further, a minimum number of coils is desired while still achieving a sinusoidal back-EMF [19]. This gives that the motor is wound with a two layers winding. The gross fill factor is imposed to be around 0.5, which is achievable with preformed tooth wound coils. The number of turns per coil is selected such that the winding accommodates parallel paths. We note:

- Line-line voltage V_{LLI} = <500 Vrms
- Phase current I_{Wrms} < 750 Arms
- Speed = 0-345 rpm (for 11,000 Nm nominal)
- Shaft power (constant torque) = 230-350 kW (S1)
- Efficiency > 95%.

The dynamic graphs for the line current, line-line EMF and instantaneous torque calculated using an analytical method (PC-BDC v10.02 [20]) is given in Fig. 6, where the finite-element analysis results are displayed in Fig. 7.

Here, the flux-density in the stator tooth and stator yoke is 1.76 T (one tooth in a group of nine for one rotor position) and the highest flux-density value (2.45 T) occurs in the stator tooth tip corner. It needs noting that this finite element analysis assumes the stator current waveform to be ideally sinusoidal.

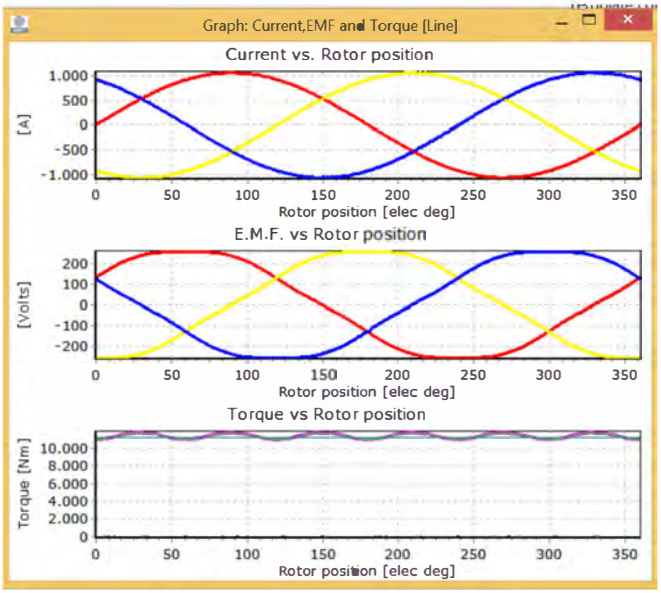

Fig. 6. Dynamic line current, line-to-line EMF and instantaneous torque of the direct-drive motor.

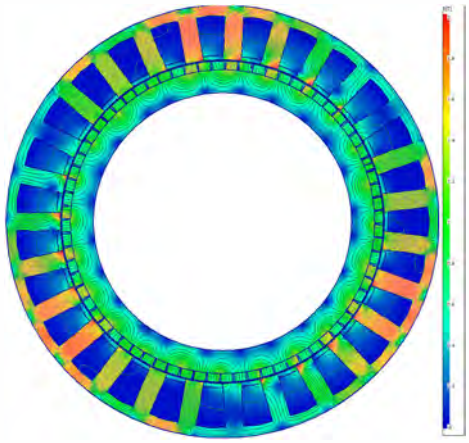

Fig. 7. Full-load finite element analysis result.

The current value that would depress the magnets beyond the 0.4 T (knee point at 180 ºC) is I_{bk} = 1842 A peak value. This is much higher than the rated current, around 925 A peak value. Albeit this short circuit current effect has still been investigated on the magnets. The value of the short-circuit current is 467 Arms. The flux-density levels within the magnets under short-circuit conditions are shown in Fig. 8. Note the minimum level of 0.43 T that occurs is at some locations within the magnets. This suggests that no parts of the magnets will be irreversible demagnetized beyond the knee point of 0.4 T if a short-circuit fault will happen. As the magnet operated well under 100 ºC, the magnets are considered to be able to withstand all the apparent demagnetization fields.

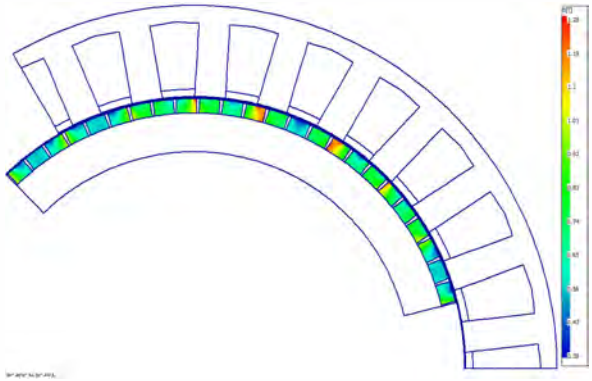

Fig. 8. Flux-density levels within the permanent magnets under short-circuit conditions.

A. *Stator copper losses*

An initial estimate of the copper loss at rated current for a machine design of a given packing factor can be derived from simple geometrical considerations of the winding:

$$P_{CU} = 3 \cdot I_{ph,rms}^2 \cdot R_{ph} = 3 \frac{J^2 Vol_{cu}}{\sigma_{cu}},$$

where R_{ph} is the phase resistance, J is the current density, Vol_{cu} is the volume of copper per are and σ_{cu} is the conductivity of copper. For this machine design, the total copper loss is 12.9 kW at 130°C above ambient. However, this is only applicable under static conditions, i.e. conditions under which current flows uniformly over the winding cross-section and the only source of current flow is the externally driven conduction current. In electric machines, it is necessary to also consider the influence of non-uniform current flow and the presence of induced eddy currents. These factors dictate that consideration must be given to constructing the winding from several parallel strands. To consider the additional copper loss due to these frequency dependent contributions three issues have been identified: non-uniform sharing of current between parallel paths; non-uniform current distribution within an individual conductor due to eddy currents; and induced eddy currents within the conductor bundle as a result of incident time-varying fields.

(i) Unequal sharing between parallel paths – A potential problem with stranded conductor bundles is that current may not flow uniformly within the parallel paths due to differences in their effective flux-linkage. This is likely to be a particular problem in this machine design since it has a relatively low number of turns per coil and open slots. Therefore, each effective turn (which will consist of various parallel strands) is distributed over a large proportion of the slot area. However, in this motor

sufficient strands are adopted to overcome the problem of non-uniformity of the conduction current.

(ii) Non-uniform current flow within each conductor – Eddy currents induced in each individual conductor can result in re-distribution of the net current flow. In extreme cases (high frequency and large conductor diameter) the net current may be restricted to a thin layer near the outer surface of the conductor, a feature which is commonly known as skin-effect. For example, for a 50 Hz supply frequency, the skin depth in copper at room temperature is ~9 mm [21]. In the design of large synchronous generators, this 9 mm skin depth is used as a basis for limiting conductor diameters to ~5-6 mm, although the exact value depends on the allowable AC copper losses, typical values being between 10-30% of the resistive losses [22]. Adopting the same guidelines for conductor maximum cross-section to skin depth as those used for large synchronous generators, then a wire diameter of ~4.0 mm has been deemed acceptable compromise.

iii) Losses generated by time-varying fields – Even with resistance limited eddy currents it may still be necessary to account for additional losses in the strands due to their exposure to a time varying field. These additional losses can be estimated using established analytical equations which are based on two main simplifying assumptions:

1. The effect of any eddy-current field re-distribution is neglected, i.e. resistance limited eddy currents. It is worth noting that the resistance limited case is a worst case in terms of losses since it neglects any decrease of the actual field due to the eddy currents reaction field.
2. The conductor diameter is small in comparison to axial length.

A pre-requisite for applying an analytical loss model to the winding is the accurate predictions of this time-varying field to which it is exposed. Since eddy current re-distribution is assumed to be negligible the time-varying field can be predicted from a series of magneto-static, non-linear, finite element field solutions over one electrical cycle. The localised time-varying magnetic flux density distribution within each element in the winding was extracted for both no-load to full-load operation. The average time-varying flux density waveform is then extracted by post-processing the finite element solutions. Having established the average flux density variation within the slot, the instantaneous power dissipation is given by [23, 24]:

$$P_{proximity} = \frac{2\pi m\, l_{stk} N_s\, N_{ph}\, d_w^{\,4} \left(2\pi f\right)^2 B_{slot}^{\,2}}{64\rho_{Cu}},$$

where m is the number of phases, l_{stk} is the stack length, N_s is the number of strands in hand, N_{ph} is the number of turns per phase, d_w is the wire diameter and B_{slot} is the average flux-density in the slot. Following, the proximity losses are included in the overall copper losses from PC-BDC by using an adjustment factor. It needs noting that the copper resistivity ρ_{Cu} includes the temperature effect. The overall proximity losses are shown from no-load to full-load in Fig. 9.

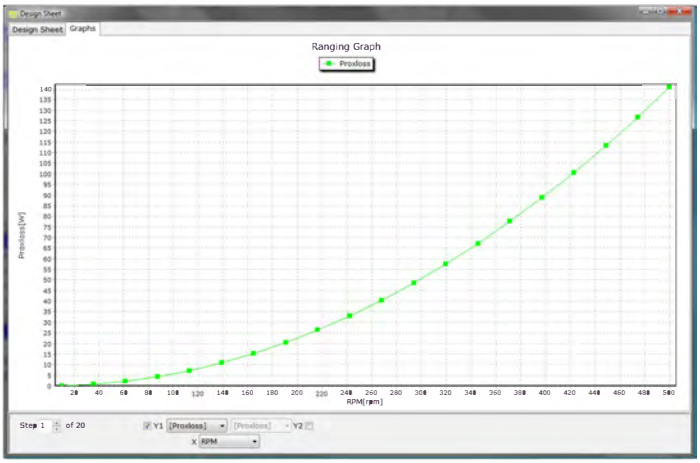

Fig. 9. Proximity losses using flux average flux density in the slot from no-load to full-load.

B. *Rotor and stator iron losses*

The low-speed nature of this application is likely to mean that stator iron loss will constitute a small proportion of the total loss. In terms of iron loss, this generator exhibits two distinctive features which will influence the selection of the stator lamination material, i.e. a high air gap flux density and low electrical frequency [25]. Of course, several methodologies for calculating iron loss in electrical machines have been proposed, including simple scaling of manufacturer's W/Kg data to a given core mass / fundamental frequency / average flux density; lumped parameter models in which the stator is divided into a limited number of regions in which average time-varying flux density waveforms are obtained and detailed finite element simulations in which sophisticated loss models are applied on an element-by-element basis to field solutions [26, 27]. Here, the iron losses are obtained using finite-element computations and afterwards an adjustment factor is applied in PC-BDC to match the analytical results with those from finite-element. This calculation assumes sinusoidal currents, i.e. no switching frequency effect, and therefore the total losses are expected to be somewhat higher than estimated (~1.5-2 times). This gives that for a standard grade 0.5 mm lamination 2.5 kW iron loss is estimated.

C. *Magnet losses*

A critical design issue in high-harmonic content PM machines, which can have a significant impact on performance, is rotor magnet loss. These magnet losses are a result of induced eddy currents in the electrically conducting rotor magnets, which in turn are generated by localised time-varying flux densities [28, 29]. In most well-designed permanent magnet machines, rotor magnet loss is considered to be a parasitic loss, as it only constitutes a relatively small proportion of the total power. However, this loss is problematic since it directly heats the magnets. This heating tends to reduce the magnet remanence and its ability to withstand demagnetisation fields. Ultimately, excessive rotor magnet loss will prevent rated power being realised. A number of design features are often incorporated into permanent magnet rotors to reduce the rotor magnet losses: rotor magnet segmentation, electrically conducting rotor screens and alternative winding configurations and phase numbers [30-32].

Here, the full-load loss is analysed using transient finite element analysis coupled to an electrical circuit. The electrical circuit consists of a three-phase inverter. The eddy-current skin depth within the magnets is 70.9 mm >> magnet thickness = 14 mm, meaning the eddy-current are resistance limited and can be estimated via analytical methods, where the magnet loss variation with speed is given in Fig. 10.

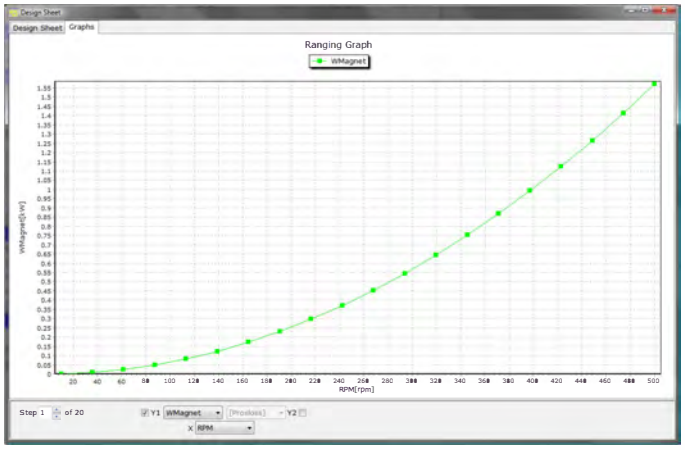

Fig. 10. Magnet losses from no-load to full-load.

IV. MOTOR THERMAL DESIGN

Accurate thermal modelling is critical to ensure that a design is viable in terms of the maximum temperature constraints. The initial sizing was performed on the basis of specifying a maximum permissible current density in the conductors, which in turn based on a-priori estimates of likely winding temperature rise for a given cooling method. The assumed current density can vary between ~3 A/mm^2 in a large naturally ventilated machine up to 25 A/mm^2 in a liquid cooled machine. Although this simplistic approach can be useful as a starting point, it is essential to establish temperature estimates on the basis of electromagnetic-thermal coupled models. Therefore, a lumped parameter equivalent thermal network approach was adopted using Motor-CAD, as shown in Fig. 11. This model employs an equivalent thermal network consisting of power sources, thermal resistances and thermal capacitances.

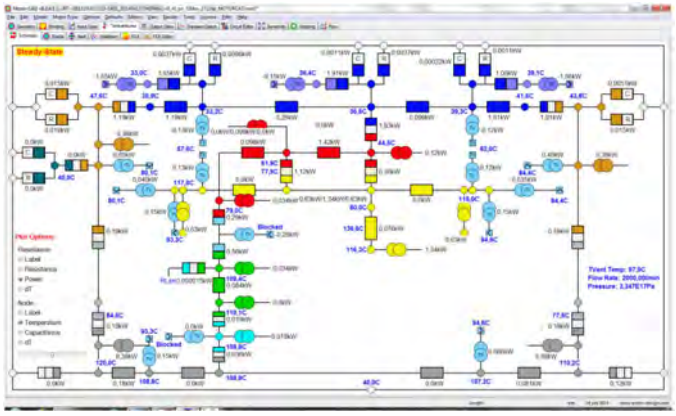

Fig. 11. Used lumped parameter model illustrating the various temperatures within the machine.

Although these lumped parameter thermal models are capable of providing accurate predictions of thermal performance, they are based on many simplifying assumptions. As such, in formulating the equivalent thermal network many of the regions are well defined, both geometrically and in terms of thermal properties, e.g. the tooth body region of the stator lamination. Hence, relatively simple analytical equations can be derived to describe the heat transfer in these regions. However, there are other regions where there is a lack of reliable material data and/or a degree of uncertainty in the exact geometries, and modelling is often reliant on published data and/or empirical guidelines. This is particularly the case for heat transfer within the conductor bundle and slot region, and at the interface between the stator lamination stack and the frame.

A typical slot region consists of the individual conductors, whose layout may or may not be precisely defined depending on the type of winding, the inter-turn voids which could be either air or some encapsulation material, and the slot-liner. The largest thermal barrier in most stator slots, particularly those in which employ encapsulation, is the slot-liner, which despite being relatively thin (~0.3 mm) has a poor thermal conductivity. In this power dense machine, the highest possible copper packing factor is used to both minimise loss and improve heat transfer within the winding, as shown in Fig. 12. In addition, the coils are impregnated with a suitable varnish (under vacuum). Vacuum enhances the heat transfer within the winding since it removes any air voids while also

improving the mechanical integrity of the winding and hence its reliability. Fig. 9 shows the temperature distribution within the slot for a model based on the above assumptions [33]. In this model a total copper loss of 480 W is generated in the region of the coil shown (this value corresponding to a rated load overall copper loss of ~13 kW for the entire machine – which consist of 27 such half coil regions).

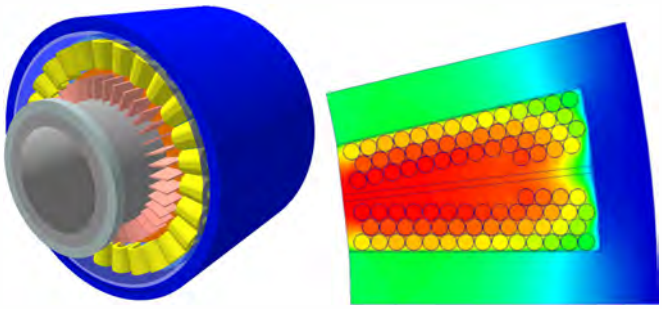

Fig. 12. 3D view of the thermal model and detailed screen shot from the slot area as solved using finite element analysis.

The heat transfer coefficient across the air gap of an electrical machine is important since a significant proportion of rotor electromagnetic losses, rotor friction losses and a smaller proportion of the stator losses are removed by the air gap flow. To improve the axial air gap air flow a fan has been mounted to the rotor shaft, which is included as illustrated in Fig. 9.

V. MOTOR PROTOTYPING

A permanent magnet machine is currently manufactured to experimentally validate the design procedure employed. The objectives of this experimental phase are to validate key findings from the modelling, particularly in terms of loss predictions, thermal modelling and influence of design features such as magnet segmentation. A back-to-back set-up is created for testing this machine with a continuous power rating of ~400 kW, with a speed range of 0-450 rpm.

Fig. 13 Rotor shaft with lamination stack and magnets showing mounting tooling.

The stacked parallel strands were wound with great care so as not to damage the insulation. The copper conductor material employed is a Temperature class H, which has a two layer insulation. A slot-liner insulation, class H with thickness 0.3 mm, was used to insulate the coil to the stator lamination and the coils individually. Fig. 13 shows the rotor with assembling tooling.

The shaft material was chosen such to provide sufficient yield strength, which permits a hollow shaft to be used to allow space for the ship's propulsion shaft. A future paper will discuss the motor and thermal verification. For example, several winding configurations have been utilized and evaluated to estimate the cost effective and thermally sufficient winding configuration, as shown in Fig. 14.

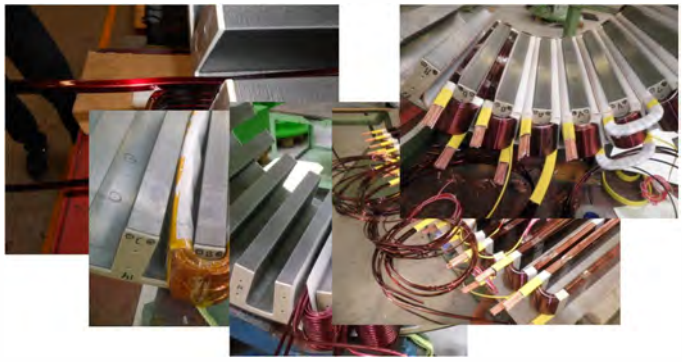

Fig. 14. Quest for the most suitable motor winding design.

VI. CONCLUSION

As cost pressures increase and environmental regulations become more stringent, the need for smart hybrid systems for inland applications will be evermore paramount. Using direct-drive PM electric machines on the propulsion shaft in these advanced drive trains allows ship-owners to take advantage of a more flexible, modular, efficient and lightweight propulsion system. This paper reports on a wide-ranging research programme into the feasibility, design, loss analysis and building of an 11,000Nm high-efficient electrical machine. This PM technology assures future-proof inland ships even considering the strictest environmental legislation. It enables ship-owners to reduce the operational costs by optimizing fuel consumption through superior efficiency, reliability and flexibility. The simple advantages of fast available power and lower fuel consumption add up to a fast return on investment and less pollution as well as higher reliability.

The paper has illustrated the importance of a concurrent engineering approach to design, which encompasses electromagnetics, power electronics, structural mechanics and thermal analysis. Indeed, although this paper is concerned with the design of an electrical machine, the key design issues and constraints

have been dictated by mechanical and thermal considerations. The electromagnetic aspects of design demonstrated the impact on the machine design of the loss and thermal modelling. The modelling and design aspects of this research will be supported by experimental measurements at component, sub-system and system level on the presented electrical machine, however this is outside the scope of this paper.

In summary, this paper has demonstrated that high-torque, low-speed permanent magnet machines pose many challenges, and that the adoption and extrapolation of design guidelines and practice from more conventional machines can lead to significant problems. As such, there are clearly still many aspects remaining which require further investigation for future large PM machines.

REFERENCES

[1] The next generation of ECO SHIP, (2002) "The Development of an electric population domestic chemical tanker, http://www.nakatani-sy.co.jp/index_er.html

[2] G.J. de Gelder, (2014) "10-15% fuel saving", http://www.groenervaren.nl/tweede-hybride-binnenvaartschip/

[3] J.M. Apsley, A. Gonzalez-Villasenor, M. Barnes, A. C. Smith, S.Williamson, J. D. Schuddebeurs, P. J. Norman, C. D. Booth, G. M. Burt, and J. R. McDonald (2009) "Propulsion drive models for full electric marine propulsion systems," IEEE Trans. Ind. Appl., vol. 45, no. 2, pp. 676–684.

[4] R.E. Hebner (2005) "Electric ship power system—Research at the University of Texas at Austin," in Proc. IEEE Electric Ship Technol. Symp., Jul. 25–27, pp. 34–38.

[5] R. Hamstra (2014) http://www.electricmarinesupport.nl/, http://www.tricoby.nl

[6] B. Zahedi, L.E. Norum, (2013) "Modeling and Simulation of All-Electric Ships With Low-Voltage DC Hybrid Power Systems", IEEE Trans. on Power Electronics, Vol. 28, No. 10, pp. 4525-4537.

[7] R. Whitney, (2013) "Ship Energy Efficiency Measures Advisory", ABS Houston USA, pp.1-72.

[8] C.N. Mueller (2011) "SISHIPCIS ECO PROP, The ECO - friendly PROPulsion for compact ships", Workshop - CO2 Emissions from Inland Navigation, Strasbourg

[9] Layman Report (2009) "ZEMSHIPS – ZERO-EMISSION SHIPS", http://ec.europa.eu, pp. 1-8.

[10] C. Sys, T. Vanelslander (2011) "Future challenges for inland navigation", University press Antwerp.

[11] "Full hybrid propulsion system diesel and electric", http://www.steyr-motors.com.

[12] C.D. Christophel (2011) "Reduzierung der CO2-Emissionen durch diesel-elektrische Antriebe am Beispiel eines bestehenden Motorgüterschiffes", Workshop CO2-Emissionen der Binnenschifffahrt, pp. 1-11.

[13] Z. Yufang, Q. Peng, Y. Hong (2013) "Fuel free ship, design for next generation", Ecological Vehicles and Renewable Energies (EVER), pp. 1-5.

[14] A. Del Pizzo, R. M. Polito, R. Rizzo, P. Tricoli (2010) "Design Criteria of On-board Propulsion for Hybrid Electric Boats", XIX International Conference on Electrical Machines, pp. 1-6.

[15] Electric Marine Support Binnenvaart B.V. (2015) "Ship schematic for Hybrid Ship", www.electricmarinesupport.nl/.

[16] S. Kuznetsov (2011) "Machine design and configuration of a 7000 HP hybrid electric drive for naval ship propulsion", IEEE International IEMDC, pp. 1625-1628.

[17] K. Boynov, J.J.H. Paulides, E.A. Lomonova (2014) "Comparative analysis of the SRM as an alternative to the PM motor for automotive applications", COMPEL, 33(5), 1599-1612.

[18] M.F.J. Kremers, J.J.H. Paulides, T.E. Motoasca, E.A. Lomonova (2013) "Analysis of a fractional slot permanent magnet machine for a series hybrid truck", COMPEL, 32(1), pp. 108-125.

[19] Y. Tang, J.J.H. Paulides, E.V. Kazmin, E.A. Lomonova (2012) "Investigation of winding topologies for permanent magnet in-wheel motors", COMPEL, 31(1), pp. 88-107.

[20] "SPEED," available on http://www.cd-adapco.com.

[21] R.L. Stoll (1974) "The analysis of eddy currents", Clarendon press, Oxford, pp. 128.

[22] A. Szucs (2001) "Macro element method for modelling eddy currents in the multi-conductor windings of electrical machines", Ph.D. thesis Helsinki university of technology.

[23] P.N. Murgatroyd, W. Farrer, R.P.D. Hodgkinson, P.D. McLoughlin, (1980) "The torroidal cage coil", IEE Proc. B, Vol. 127 , pp. 207-214.

[24] C.R. Sullivan (1999) "Winding Loss Calculation with Multiple Windings, Arbitrary Waveforms and Two-Dimensional Field Geometry", Industry Applications Conference, Vol. 3 pp. 2093-2099.

[25] J.J.H. Paulides, K.J. Meessen, E.A. Lomonova (2008) "Eddy-current losses in laminated and solid steel stator back iron in a small rotary brushless permanent-magnet actuator", IEEE Transactions on Magnetics, 44(11), pp. 4373-4376.

[26] A.J. Moses, G.H. Shirkoohi (1987) "Iron loss in non-oriented electrical steels under distorted flux conditions", IEE Trans. on Magnetics, Vol 23, No 5, pp 3127-3220.

[27] T. Yamaguchi, K. Narita (1976) "Rotational power losses in commercial Silicon-Iron laminations", Electrical Eng. In Japan, Vol. 96, No 4, pp 15-21.

[28] J.J.H. Paulides (2005) "High performance 1.5MW 20,000rpm permanent magnet generator with uncontrolled rectifier for 'more-electric' ship applications", PhD thesis, University of Sheffield.

[29] J. Jacob, J.J.H. Paulides, E.A. Lomonova, (2014) "Influence of rotor design on performance of PM machines for heavy-duty traction applications", COMPEL, 33(5), pp. 1541-1557.

[30] N. Taghizadeh Irenji, S.M. Abu Sharkh, M.R. Harris (2000) "Effect of rotor sleeve conductivity on rotor eddy-current loss in high-speed PM machines", ICEM Espoo Finland, pp. 645-648.

[31] J.L.F. Van der Veen, L.J.J. Offringa, A.J.A. Vandenput (1997) "Minimising rotor losses in high-speed high-power permanent magnet synchronous generators with rectifier load", IEE Proc Electrical Power applications, Vol. 144, No. 5, pp. 331-337.

[32] E. Bunzel, G. Mueller (1991) "General analysis of a 6-phase synchronous machine", Int. conf. Evolution and modern aspects of synchronous machines, pp. 333-340.

[33] "Motor-CAD and Motor-LAB," available on www.motor-design.com.